International Journal of Engineering Inventions
e-ISSN: 2278-7461, p-ISSN: 2319-6491
Volume 13, Issue 4 [April. 2024] PP: 202-216

Contribution in the Modelling, the Analysis and the Application of the Robust Control System for an Aerogenerator Double Feed Asynchronous Machine Type

RANDRIANAMBININTSOA Manitra Léon [1]
Electrical Engineering, ED-STII, Université d'Antananarivo Madagasikara
RABEARIVELO Apotheken Gericha [2]
Electrical Engineering, ED-STII, Université d'Antananarivo Madagasikara
RANDRIAMITANTSOA Andry Auguste [3]
TASI, ED-STII, Université d'Antananarivo Madagasikara
[1] *Ph.D. Student, GE, ED-STII, Université d'Antananarivo Madagasikara, e-mail:* manitraleon@gmail.com
[2] *Thesis Co-Director, GE, ED-STII, Université d'Antananarivo Madagasikara, e-mail:* gericha407@gmail.com
[3] *Thesis Director, TASI, ED-STII, Université d'Antananarivo Madagasikara, e-mail:* Andry.randriamitantsoa@univ-antananarivo.mg

ABSTRACT: *This article presents the research results of a DFIM behavior (Double Fed Induction Machine), for the electrical energy production by a wind turbine generator system, by integrating directly its model, its direct simulation in order to present its behavior, to make tuning and present the desired behavior. The objectives being to contribute to its modeling, then to control and analyze a DFIM type wind turbine generator for applying the robust control multivariable system. In a brief way, the essential aim is to control the machine for generate electrical energy by controlling the powers with the currents and voltages rotor, while regulating its speed rotation.*

Date of Submission: 15-04-2024 Date of acceptance: 28-04-2024

NOMENCLATURE

Lower-case letters normal

Symbol	Description	Unit
e_{ind}	Rotor induced electromotive force	V
f_r	Rotor frequency	Hz
f_s	Stator frequency	*Hz*
i_{in}	Converter input current	*A*
i_{sd} and i_{sq}	*dq* synchronous armature stator courant references	*A*
i_{red} and i_{req}	Grid current rectifier side in *dq* references	*A*
i_{rabc}	Rotor three phase current	*A*
i_{sabc}	Stator three phase current	*A*
p	Poles pairs	
s	slip	*%*
$u_1$and u_2 , u_3 and u_4	*Arbitrary proportionality coefficient of from dq components in to triphase system*	
v_{rd} et v_{rq}	*dq* synchronous armature rotor voltage references	*V*
v_{sd} et v_{sq}	*dq* synchronous armature stator voltage references	*V*
v_{rabc}	Three phase rotor voltage	*V*

v_{sabc}	Three phase stator voltage	*V*

Upper-case letters normal

Symbol	**Description**	**Unit**
C	Capacitor	*F*
J	Load-rotor inertia moment	$Kg.m^2$
F	Viscous friction coefficient	*%*
L_r	Rotor inductance	*H*
L_s	Stator inductance	*H*
M_{sr}	Mutual inductance rotor-stator	*H*
P_r	Rotor active power	*W*
P_s	Stator active power	*W*
Q_r	Rotor reactive power	*VAR*
Q_s	Stator reactive power	*VAR*
M_{sr}	Mutual inductance	*H*
R_r	Rotor resistance	**Ω**
R_s	Stator resistance	**Ω**
T_L	Load torque	*Nm/rad*
T_{em}	Electromagnetic torque	*Nm/rad*
V_r	Rotor supply voltage	*V*
V_s	Stator efficient voltage	*V*

Greek letters

Symbol	**Description**	**Unit**
ϕ_{rd} et ϕ_{rq}	*dq* synchronous armature rotor flux references	*Wb*
ϕ_{sd} and ϕ_{sq}	*dq* synchronous armature stator flux references	*Wb*
ω_r	Current and voltage electrical pulsation rotor winding	*rad/s*
ω_s	Current and voltage electrical pulsation stator winding	*rad/s*
ω_m	Rotor mechanical speed rotation	*rad/s*

I. INTRODUCTION

In the current era, the performance and reliability of wind energy, as well as the continuity of its service, should replace the production of old-fashioned electrical energy which is increasingly creating climatic destabilization phenomena due to the polluting gases emission. One of the more specific configurations of variable speed wind turbines, uses the asynchronous double fed machine, referred to by the abbreviation DFIM or MADA (Machine Asynchrone à Double Alimentation) in French. The figure 1 represents the DFIM general control strategy.

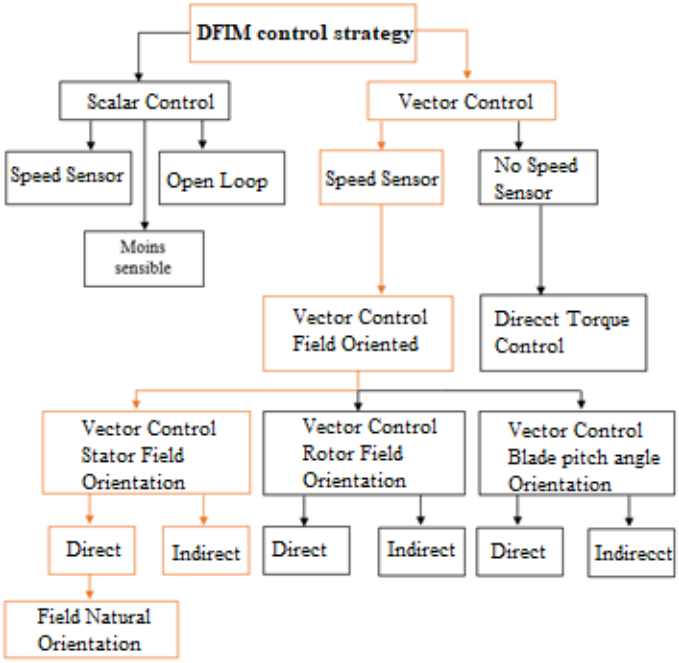

Figure 1 : Double feed induction machine general control strategy.

Many of the DFIM control strategies have been proposed in literature. The problem of the DFIM control strategy has been dealt with using different approaches. The DFIM oriented field control, with and without speed sensor, has been presented (Metwally et al. (2002) and EL Khil de Khojet et al. 2004). The lack tolerance of the DFIM command has been studied under time-varying conditions (Gritli et al. 2011). Other control strategies including direct torque control (Bonnet et al. 2007), sliding-mode control (Vidal et al. 2008), output-feedback control (Peresadaa et al. 2004) , and closed loop control (Salloum et al. 2007) [1].

II. PROBLEM'S PRESENTATION

2.1. System control model

The machine is controlled to generate electrical energy by controlling the powers, by the rotor currents and voltages, while regulating its rotation speed. The call of tools for solving mathematical differential equations allows modeling of machine dynamics under differential equations systems. We have the following parameters, [2] [3]:

$$\gamma_1 = \frac{R_r L_s^2 + R_s M_{sr}^2}{\sigma L_r L_s^2}, \qquad \gamma_2 = \frac{M_{sr}}{\sigma L_s L_r}, \qquad \gamma_3 = \frac{1}{\sigma L_r}, \quad \sigma = 1 - \frac{M_{sr}^2}{L_s L_r}, \qquad \tau_s = \frac{L_s}{R_s}$$

$$v_{rd} = u_1 v_{dc}, v_{rq} = u_2 v_{dc} \qquad i_e = u_1 i_{rd} + u_1 i_{rq} \qquad i_{ot} = u_3 i_{red} + u_4 i_{req}$$

$$
\begin{cases}
\dfrac{d\omega_m}{dt} = -\dfrac{F}{J}\omega_m - p\dfrac{M_{sr}}{JL_s}\left(\phi_{sd}i_{rd} - \phi_{sd}i_{rq}\right) - \dfrac{T_L}{J} \\
\dfrac{di_{sd}}{dt} = -\gamma i_{sd} + \omega_s i_{sq} + p\omega_m \dfrac{M_{sr}}{\sigma L_s L_r}\phi_r + \dfrac{1}{\sigma L_s}v_{sd} \\
\dfrac{di_{sq}}{dt} = -\gamma i_{sq} + \omega_s i_{sd} + p\omega_m \dfrac{M_{sr}}{\sigma L_s L_r}\phi_r + \dfrac{1}{\sigma L_s}v_{sq} \\
\dfrac{di_{rd}}{dt} = -\gamma_1 i_{rd} + \left(\omega_s - p\omega_m\right)i_{rq} + \dfrac{\gamma_2}{\tau_s}\phi_{sq} - p\gamma_2\omega_m\phi_{sq} - \gamma_2 V_s \\
+ \gamma_3 v_{dc}u_1 \\
\dfrac{di_{rq}}{dt} = -\gamma_1 i_{rq} - \left(\omega_s - p\omega_m\right)i_{rd} + \dfrac{\gamma_2}{\tau_s}\phi_{sq} + p\gamma_2\omega_m\phi_{sd} \\
+ \gamma_3 v_{dc}u_2 \\
\dfrac{dv_{dc}}{dt} = \dfrac{1}{C}\left(u_3 i_{red} + u_4 i_{req} - i_e\right) \\
\dfrac{di_{red}}{dt} = \omega_s i_{req} + \dfrac{V_s}{L_0} - \dfrac{v_{dc}u_3}{L_0} \\
\dfrac{di_{req}}{dt} = -\omega_s i_{red} - \dfrac{v_{dc}u_4}{L_0}
\end{cases}
\tag{1}
$$

Possibilities control of the machine are presented in figure 2.

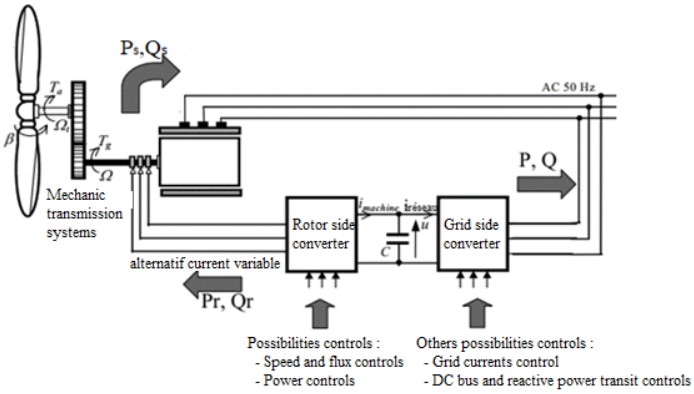

Figure 2: The different possibilities control of the machine

2.2. Double feed asynchronous machine model

First of all, we can summarize below according the generalities double feed asynchronous machine multivariable control, in generator operating.

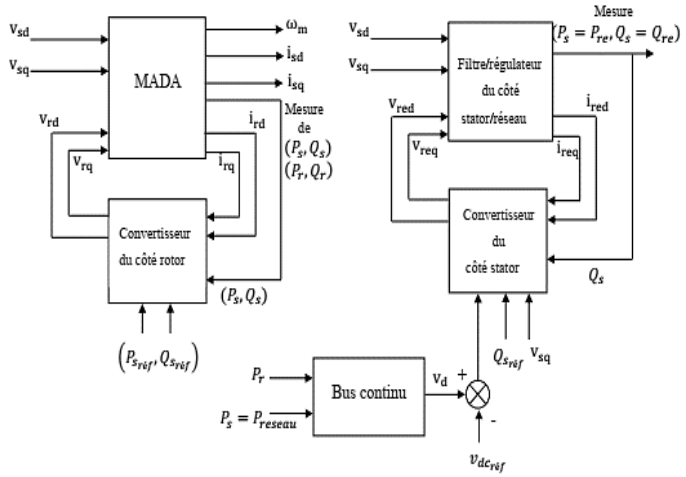

Figure 3: Diagram detailed form

The state space model of the machine in the virtual referential (dq) with the armature tension orientation is,

$$\frac{d\dot{x}(t)}{dt} = \begin{bmatrix} -\frac{F}{J} & 0 & 0 & p\frac{M_{sr}\phi_{sq}}{JL_s} & -p\frac{M_{sr}\phi_{sd}}{JL_s} & 0 & 0 & 0 \\ p\frac{M_{sr}\phi_{rq}}{\sigma L_s L_r} & -\gamma & \omega_s & 0 & 0 & 0 & 0 & 0 \\ 0 & -\omega_s & -\gamma & 0 & 0 & 0 & 0 & 0 \\ -p\gamma_2\phi_{sq} & 0 & 0 & -\gamma_1 & -p\omega_s(1-s)+\omega_s & 0 & 0 & 0 \\ -p\gamma_2\phi_{sd} & 0 & 0 & p\omega_s(1-s)-\omega_s & -\gamma_1 & 0 & 0 & 0 \\ 0 & 0 & 0 & 0 & 0 & 0 & \frac{u_3}{C} & \frac{u_4}{C} \\ 0 & 0 & 0 & 0 & 0 & -\frac{u_3}{L_0} & 0 & \omega_s \\ 0 & 0 & 0 & 0 & 0 & -\frac{u_4}{L_0} & -\omega_s & 0 \end{bmatrix} \cdot \begin{bmatrix} \omega_m \\ i_{sd} \\ i_{sq} \\ i_{rd} \\ i_{rq} \\ i_{in} \\ i_{red} \\ i_{req} \end{bmatrix}$$

$$+ \begin{bmatrix} 0 & 0 & 0 & 0 & 0 & 0 & 0 & 0 \\ 0 & \frac{1}{\sigma L_s} & 0 & 0 & 0 & 0 & 0 & 0 \\ 0 & 0 & \frac{1}{\sigma L_s} & 0 & 0 & 0 & 0 & 0 \\ 0 & 0 & -\frac{M_{sr}}{\sigma L_s L_r} & \frac{1}{\sigma L_r} & -\frac{M_{sr}}{\sigma L_s L_r} & 0 & 0 & 0 \\ 0 & 0 & 0 & 0 & \frac{1}{\sigma L_r} & 0 & 0 & 0 \\ 0 & 0 & 0 & 0 & 0 & -\frac{1}{C} & 0 & 0 \\ 0 & 0 & \frac{1}{L_0} & 0 & 0 & 0 & 0 & 0 \\ 0 & 0 & 0 & 0 & 0 & 0 & 0 & 0 \end{bmatrix} \cdot \begin{bmatrix} 0 \\ v_{sd} \\ v_{sq} \\ v_{rd} \\ v_{rq} \\ v_{dc} \\ 0 \\ 0 \end{bmatrix}$$

$$y(t) = \begin{bmatrix} 1 & 0 & 0 & 0 & 0 & 0 & 0 & 0 \\ 0 & 1 & 0 & 0 & 0 & 0 & 0 & 0 \\ 0 & 0 & 1 & 0 & 0 & 0 & 0 & 0 \\ 0 & 0 & 0 & 1 & 0 & 0 & 0 & 0 \\ 0 & 0 & 0 & 0 & 1 & 0 & 0 & 0 \\ 0 & 0 & 0 & 0 & 0 & 1 & 0 & 0 \\ 0 & 0 & 0 & 0 & 0 & 0 & 1 & 0 \\ 0 & 0 & 0 & 0 & 0 & 0 & 0 & 1 \end{bmatrix} \begin{bmatrix} \omega_m \\ i_{sd} \\ i_{sq} \\ i_{rd} \\ i_{rq} \\ v_{dc} \\ i_{red} \\ i_{req} \end{bmatrix} \quad (2)$$

2.3. Double feed asynchronous machine robust control

The parameters of the system are blemished of parametric uncertainty. Every coefficient uncertain $\tilde{p}_i$ is modeled as:

$$\tilde{p}_i = p_i(1 + \omega_i\delta_i)\ , |\delta_i| < 1 \quad (3)$$

Where $\tilde{p}_i$ is the nominal value of the considered parameter and ω_i, the corresponding weighting coefficient, and δ_i the uncertainty. We chose $\omega_i = 0.1$ for all parameters. By the superior linear fractional transformation, [6], [7] we have:

$$\tilde{p}_i = [Q_{22} + Q_{21}\Delta_u(I - Q_{11}\Delta_u)^{-1}Q_{12}] \quad (4)$$

Where $Q_i = \begin{bmatrix} 0 & p_i \\ \omega_i & p_i \end{bmatrix}$.

When considering the error model among the direct additive shape for corrector synthesis. We consider like a weighting function the scalar functions, [6], [7].

$$W_u = 5 \times 10^{-4}\frac{(s+1)}{(s+1)} \qquad W_p = 4 \times 10^{-7}\frac{(0.1s+1)}{(5s+100)}$$

To reach the wanted performance, it is necessary to satisfy the inequality$\|W_u(I+GK)^{-1}\|_\infty < 1$. Here, the weighting function is a scalar function, then the singular values of the sensitivity function$(I + G_{lo}K_{lo})^{-1}$, on all of the frequency range must be gotten by the curve of $\frac{1}{W_u}$. It means that $\|W_u(I+GK)^{-1}\|_\infty < 1$ if and only if all frequencies$[(I+GK)^{-1}(jw)] < \left|\frac{1}{W_u(jw)}\right|$.

Let considers the interconnection matrix of the open loop P and the transfer matrix closed loop M:

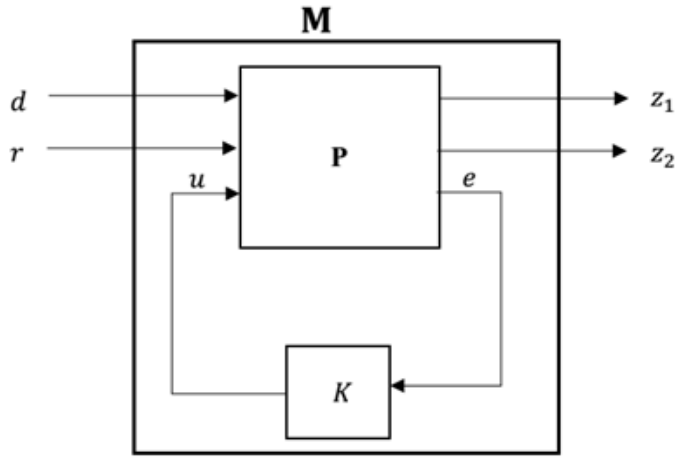

Figure 4 : Bloc diagram for the P and M matrices distinction

While doing the calculation, the corrector K, after the $\|H\|_\infty$ synthesis,

$$K = \begin{bmatrix} K_{11} & K_{12} \\ K_{21} & K_{22} \end{bmatrix}$$

$$K_{11} = \frac{\begin{array}{l}-6.11.10^{21}s^7 - 3.67.10^{28}s^6 - 7.35.10^{34}s^5 - 4.89.10^{40}s^4 - \\ 3.02.10^{42}s^3 - 4.88.10^{45}s^2 - 4.75.10^{45}s - 2.39.10^{44}\end{array}}{\begin{array}{l}s^8 + 8.64.10^{12}\,s^7 + 7.93.10^{19}s^6 + 3.03.10^{26}s^5 + 3.4.10^{32}s^4 + \\ 7.63.10^{37}s^3 + 2.66.10^{42}s^2 + 4.76.10^{46}\,s + 4.38.10^{46}\end{array}}$$

$$K_{12} = \frac{\begin{array}{l}1.36.10^{9}s^7 + 1.17.10^{22}s^6 + 8.09.10^{28}s^5 + 2.22.10^{35}s^4 + \\ 8.61.10^{37}s^3 + 2.55.10^{42}s^2 + 4.53.10^{46}s + 4.16.10^{46}\end{array}}{\begin{array}{l}s^8 + 8.64.10^{12}\,s^7 + 7.93.10^{19}s^6 + 3.03.10^{26}s^5 + 3.4.10^{32}s^4 + \\ 7.63.10^{37}s^3 + 2.66.10^{42}s^2 + 4.76.10^{46}\,s + 4.38.10^{46}\end{array}}$$

$$K_{21} = \frac{\begin{array}{l}4.3.10^{15}s^7 + 2.6.10^{22}s^6 + 5.27.10^{28}s^5 + 3.65.10^{34}s^4 + \\ 1.38.10^{39}s^3 + 2.67.10^{43}s^2 + 2.59.10^{47}s + 2.79.10^{48}\end{array}}{\begin{array}{l}s^8 + 8.64.10^{12}\,s^7 + 7.93.10^{19}s^6 + 3.03.10^{26}s^5 + 3.4.10^{32}s^4 + \\ 7.63.10^{37}s^3 + 2.66.10^{42}s^2 + 4.76.10^{46}\,s + 4.38.10^{46}\end{array}}$$

$$K_{22} = \frac{\begin{array}{l}2.84.10^{6}s^7 + 2.46.10^{19}s^6 + 1.75.10^{26}s^5 + 5.03.10^{32}s^4 + \\ 1.04.10^{38}s^3 + 3.66.10^{42}s^2 + 6.61.10^{46}s + 1.55.10^{46}\end{array}}{\begin{array}{l}s^8 + 8.64.10^{12}\,s^7 + 7.93.10^{19}s^6 + 3.03.10^{26}s^5 + 3.4.10^{32}s^4 + \\ 7.63.10^{37}s^3 + 2.66.10^{42}s^2 + 4.76.10^{46}\,s + 4.38.10^{46}\end{array}}$$

III. SIMULATION DIAGRAM

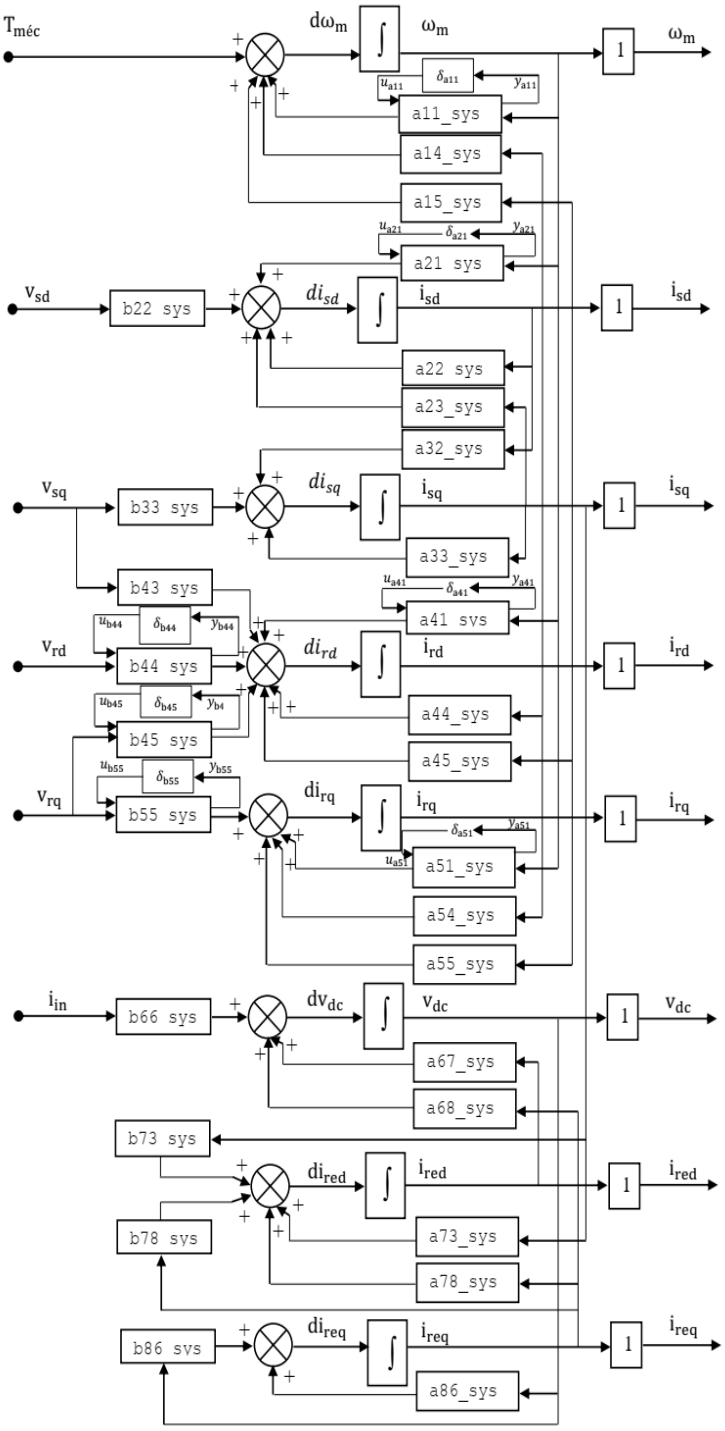

Figure 5 : Disturb system bloc diagram

IV. RESULTS:

Double feed asynchronous generator robust control and µ-synthesis

4.1 Disturbed system analysis with unstructured uncertainties

The diagram block for analyzing the system with unstructured uncertainties is represented on the figure 6:

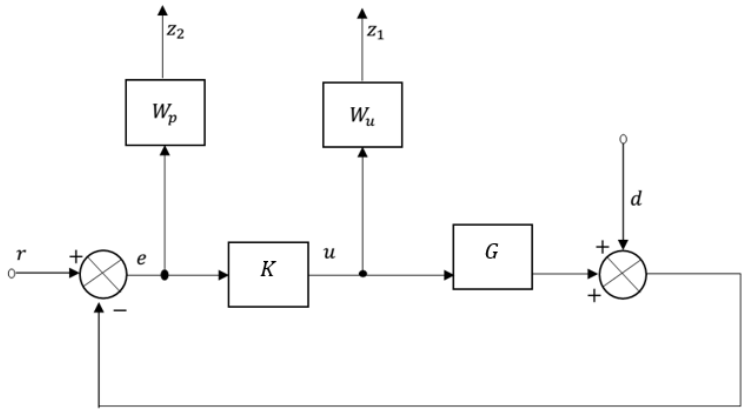

Figure 6: Disturbed system diagram block with non-structured uncertainties

a. Stability

The norm's curve$\|M_{rs}\|_\infty$, designates the robust stability with the direct additives errors form model is represented within the next figure, so that:

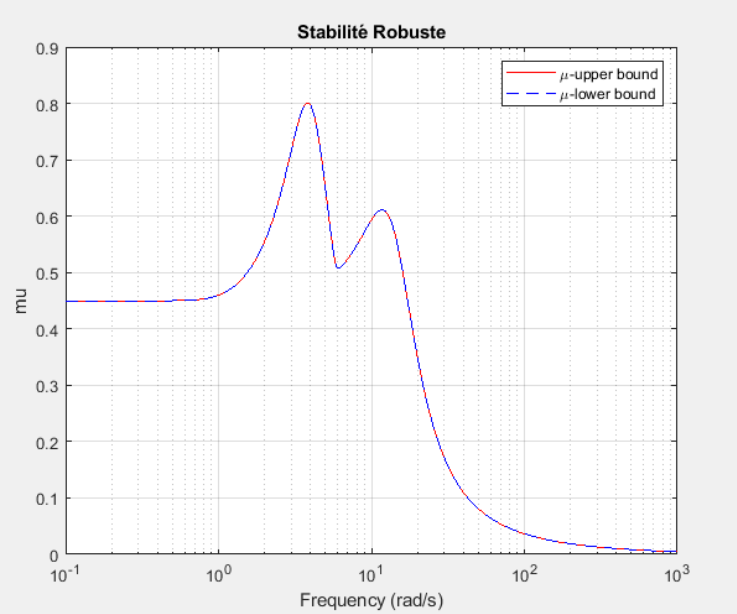

Figure 7 : Control system robust stability

According to this figure 7, we can say on the robust stability analysis, that the system is said steady robust because$\max[\mu(M_{11})] < 1$. The robust stability is assured although the uncertainty of the model.

b. Performance

The upper and lower frequency response of the singular value of the unstructrured matrix *M*, the matrix analysis system performance robust for the corrector is graphically represented in figure 8.

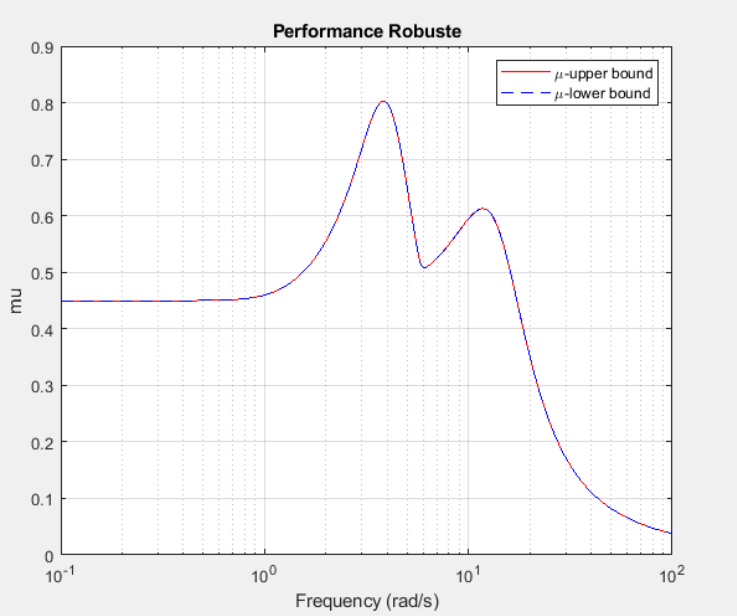

Figure 8 : Performance robuste du système asservi

The system responds to the robust performance criteria as showing the following figure 8. According to the analysis, the performance is assured with the corrector by the H_∞ synthesis, because $\max[\mu(M_{22})] < 1$. The uncertain system assures its robust performance in relation to the uncertainties of the model.

4.2 Disturbed system analysis with structured uncertainties

The diagram block for analyzing the system with structured uncertainties is represented on the figure 9:

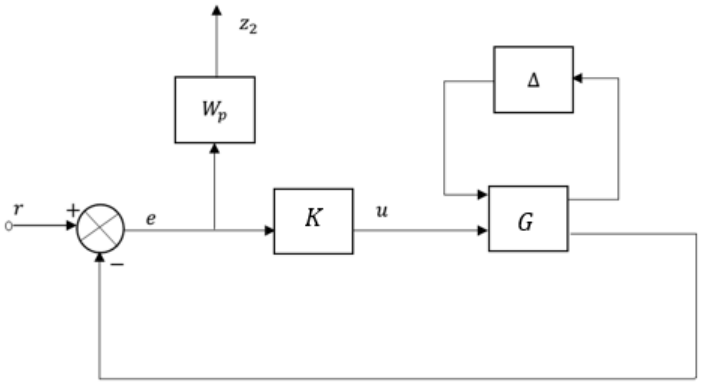

Figure 9: Disturbed system diagram block analysis with structured uncertainties

a. Stability

The norm's curve$\|M_{rs}\|_\infty$, designates the robust stability with structured form model is represented within the next figure, so that:

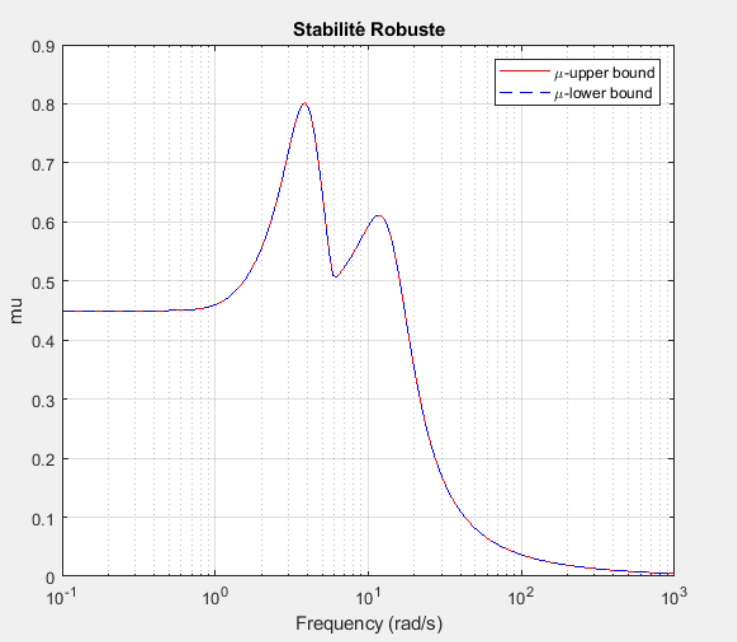

Figure 8 : **Closed-loop system robust stability**

According to the figure, we can tell on the robust stability analysis, that the system is judged steady robust because $\max[\mu(M_{11})] < 1$.

b. Performance

The upper and lower frequency response of the singular value of the structrured matrix *M*, the matrix analysis system performance robust for the corrector is graphically represented in figure 10.

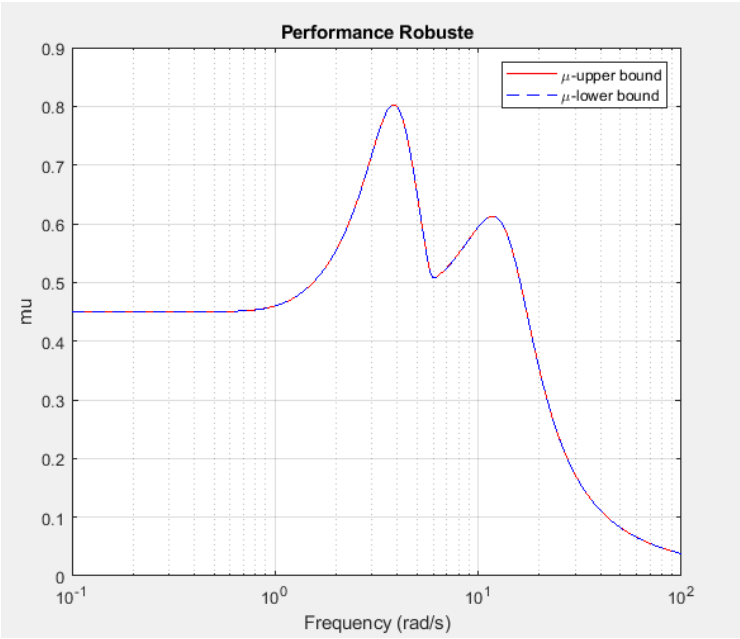

Figure 10 : System's robust performance

According to the figure, we can tell on the robust stability analysis, that the system is judged steady robust because $\max[\mu(M_{22})] < 1$.

The uncertain system assures the robust in performance to the modeled uncertainty. The compromise of uncertainty of the model and gain of the system is effective even to a level of 219% of the uncertainty modeled. This value of 219% can lead to a $\max[\mu(M_{22})] = 0.456 < 1$ to 14.3 [rad/s].

4.3 Disturbed system analysis with structured and unstructured uncertainties

The diagram block for analyzing the system with structured and unstructured uncertainties is represented on the figure 11:

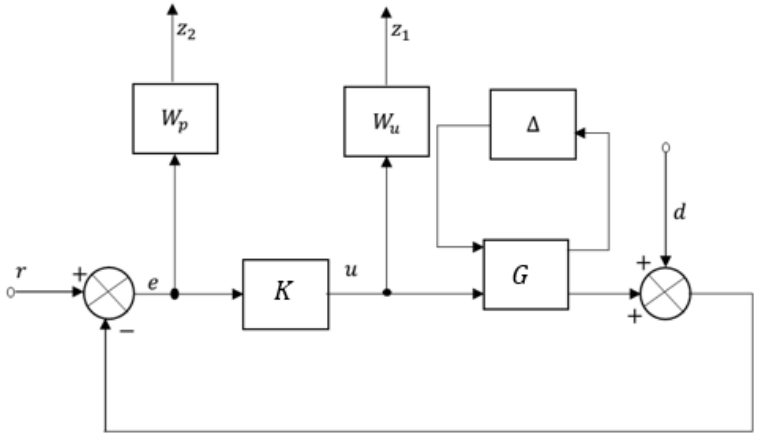

Figure 11 : Unstructured and structured uncertainties system

a. Stability

The norm's curve$\|M_{11}\|_\infty$, designates the robust stability with unstructured and structured form model is represented within the next figure, so that:

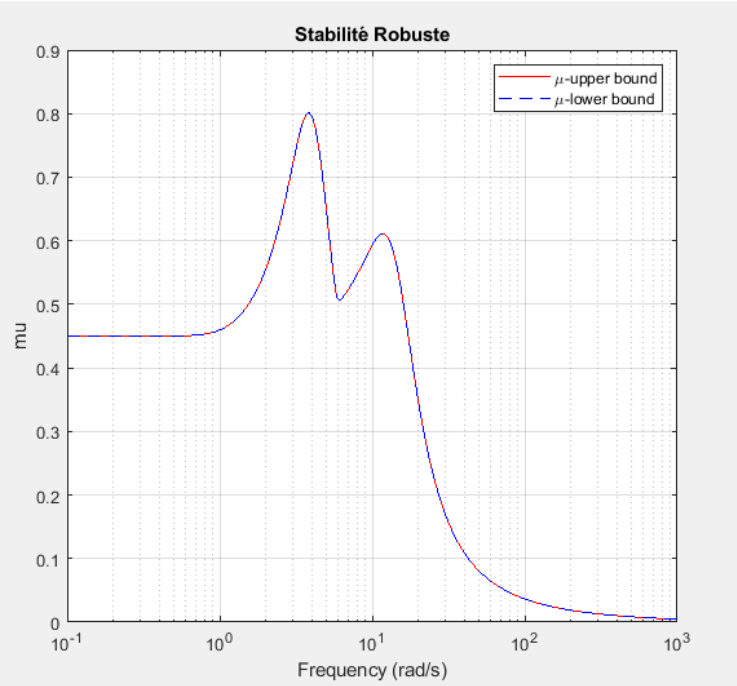

Figure 12 : Closed-loop system robust stability

According to the figure, we can tell on the robust stability analysis, that the system is judged steady robust because $\max[\mu(M_{11})] < 1$.

As the nominal system is always steady, the uncertain system assures the robust performance in relation to the modeled uncertainty. The compromise between uncertainty of the model and gain of the system is always steady to a level of 123% of the uncertainty modeled, after simulation under MatLab.

b. Performance

The upper and lower frequency response of the singular value of the structrured and unstructured matrix *M*, the matrix analysis system performance robust for the corrector is graphically represented in figure 13

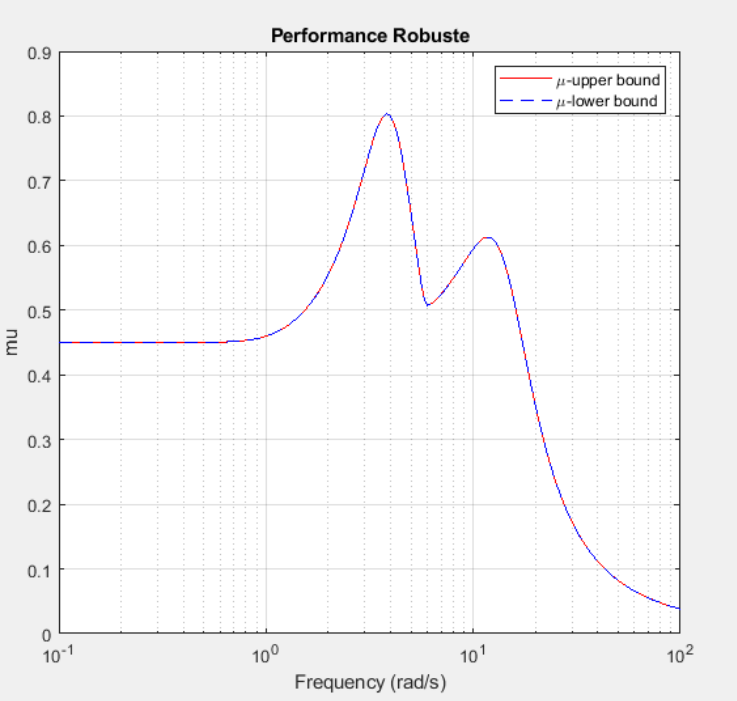

Figure 13 : **System's robust performance**

According to the figure, we can tell on the robust stability analysis, that the system is judged steady robust because $\max[\mu(M_{22})] < 1$.
The robust control systems mutlivariables theory application to the double feed asynchronous generator permits to achieve the presented below results, according to the following numerical data [1]:

Synchronous speed [*tr/min*]	1500
Rated power [*kW*]	2000
Stator voltage/line voltage [V_{rms}]	690
Stator current [A_{rms}]	1760
Torque [*Nm*]	12732
Stator connection	star
p	2
u	0.34
R_s [Ω]	2.6
$L_{\sigma s}$ [H]	0.087
L_m [mH]	2.5
$R_r^{'}$ [mΩ]	26.1
$L_{\sigma r}^{'}$ [mH]	0.738
R_r [mΩ]	2.9
$L_{\sigma r}$ [mH]	0.087
L_s [mH]	2.587
L_r [mH]	2.587

- The DFIG functions in generator operation, confronted to the different conditions of functioning, according to the parameters of the wind speeds. We present the nominal torque.

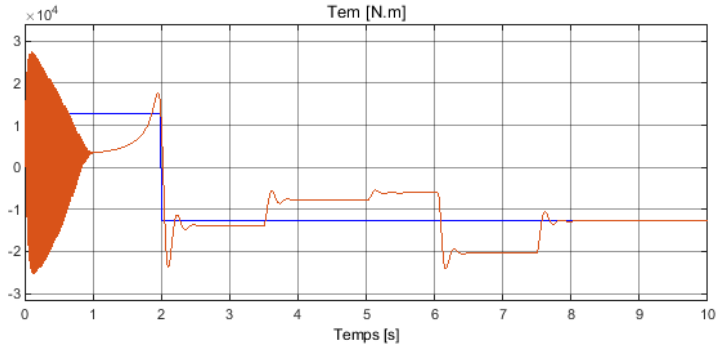

Figure 14 : Electromagnetic torque parameterized according to the wind speed variation

- On this figure 14, we have the speed generator behavior, whatever is the wind speed variation, and the generator rotation speed is never moves away enough far from the rated speed (always to the surroundings of 157.14 rad /s or 1500 in rpm).

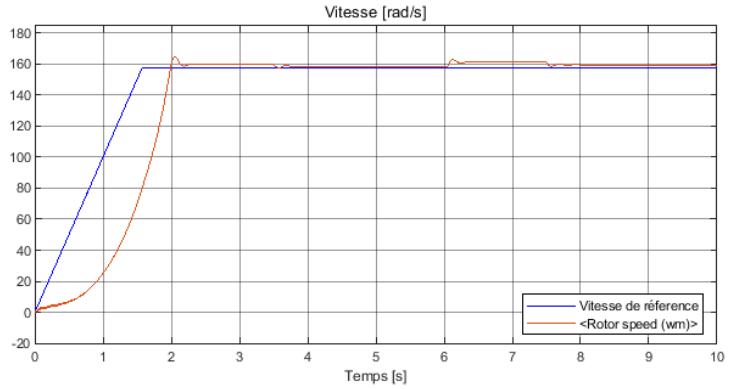

Figure 15 : Double feed asynchronous generator speed curves parameterized by the wind speed variations

We represent by the following figure 18, the stator currents *dq* behavior

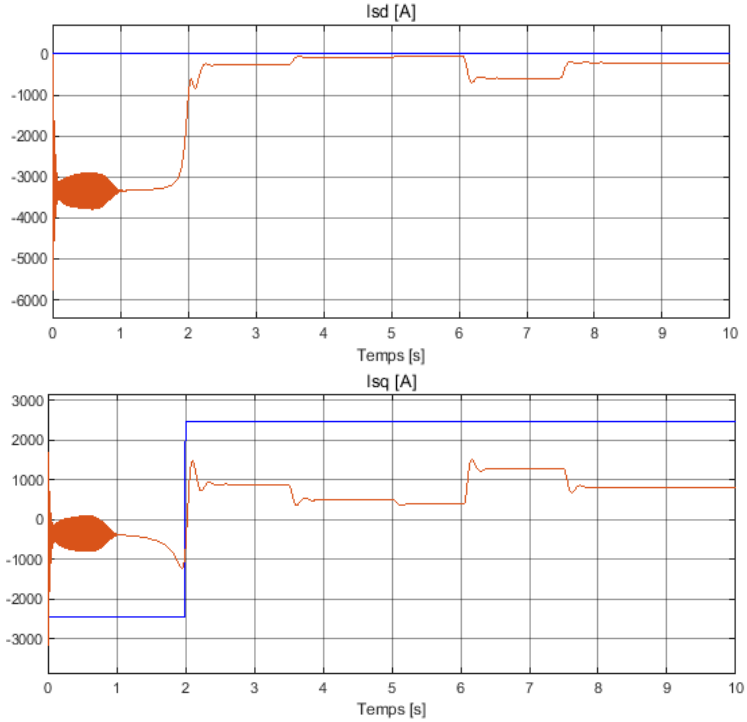

Figure 16 : Stator currents *dq* behavior according to the wind speed variations

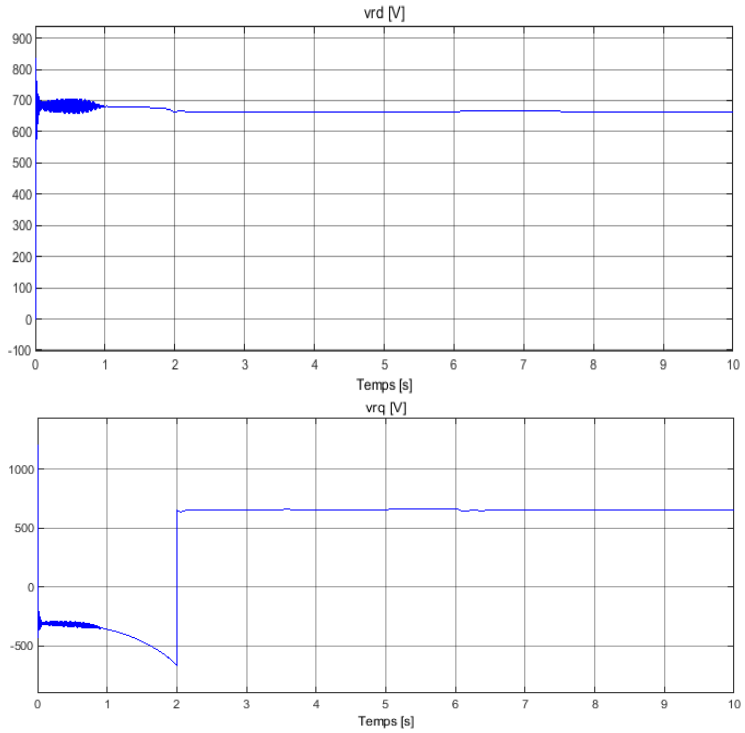

Figure 17 : *dq* voltages control behavior

In this figure, the rotor three phase currents is represented, the amplitude and the frequency of these currents vary according to the values of the wind speed variations.

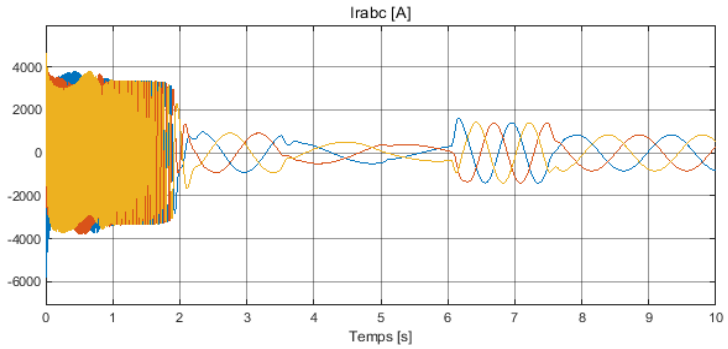

Figure 18 : Rotor current frequency and amplitude variations parameterized according the wind speed variations

On the other hand, on the figure 18, the stator three phase currents is represented, the amplitude of these currents varies according to the values of the wind speed variations, but the frequency remains unaltered (always constant).

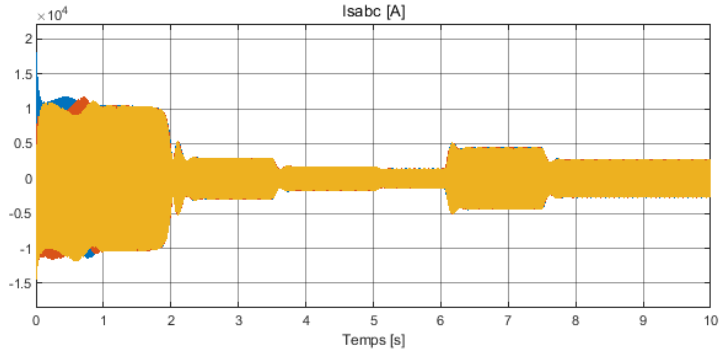

Figure 19 : Stator current frequency and amplitude variations parameterized according the wind speed variations

Whatever is the variations of the different features and parameters of its working, tensions gotten to the level of the stator (output) have the same frequencies always that the currents of the network, and the amplitudes always follow the values of order or reference.

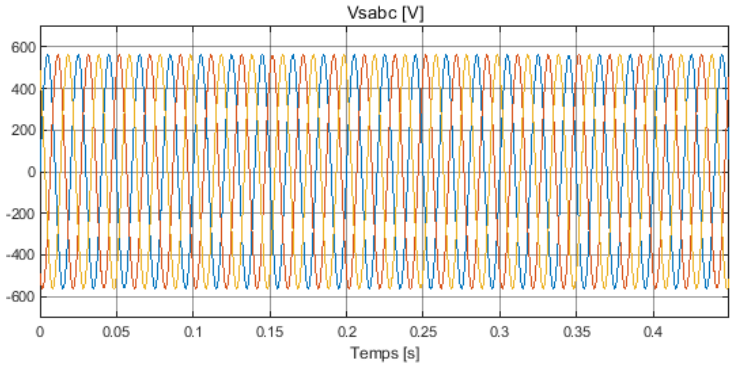

Figure 9 : Stator level voltage parameterized by the wind speeds

V. CONCLUSION

The double feed asynchronous machine specificity the is demonstrated [11], [12] according to these results presented by these figures, simulated under MATLAB, they show that if we want to control the system, of a manner to that when wind blows to very elevated speeds, a regulator will maintain the speed of the turbine in the maximal speed range game that the machine could support. And if the speed of wind is much reduced, a sensor will ask to the system to provide a current via the network or an electric power generator to make turn the machine while giving a régime of speed so that the turbine can remain in the minimal speed range game.

REFERENCES

[1]. G. ABAD, J. LÓPEZ, A. MIGUEL RODRÍGUEZ, L. MARROYO, G. IWANSKI,. Doubly fed induction machine, modeling and control for wind energy generation. Ieee Series, 2016.
[2]. X. DEHONG, F. BLAABJERG, C. WENJIE, and N. ZHU. Advanced Control of Doubly Fed Induction Generator for Wind Power Systems, First Edition. © 2018 by The Institute of Electrical and Electronics Engineers, Inc. Published 2018 by John Wiley & Sons, Inc.
[3]. GIRI, FOUAD. Ac electric engine control advanced design of techniques and applications. 2013.
[4]. IWANSKI, Gonzalo. A. (2014). Properties and control of a doubly fed induction machine in Power Electronics for Renewable Energy Systems, Transportation and Industrial Application. John Wiley & Sons
[5]. N. PHUNG QUANG and J.-A. DITTRICHN, Vector Control of Three-Phase AC Machines,
[6]. F. LIN, Robust Control Design, an Optimal Control Approach, 2007
[7]. Da-Wei GU, P. H. PETKOV M. M. KONSTANTINOV, Robust Control Design with MATLAB®, 2013
[8]. G. Rigatos, Intelligent Renewable Energy Systems, © Springer International Publishing Switzerland 2016
[9]. RABEARIVELO Apotheken Gericha, Université d'Antananarivo, Contribution à la modélisation, à la commande robuste, à la mu-analyse des rotors et des systemes de vol d'helicoptere, 2018
[10]. RANARISON Solofo Herizo, Université d'Antananarivo, Contribution a la modélisation, à la commande robuste et à la mu-analyse à temps continu d'un avion souple, 2018
[11]. Hubert Razik, Handbook of Asynchronous Machine with Variable Speed, 2011
[12]. ZHOU, DAO, SONG, YIPENG; BLÅBJERG, FREDE. Modern control strategies of doubly-fed induction generator based wind turbine system, Published in: Chinese Journal of Electrical Engineering, 2016